Inorganic Chemistry

pubs.acs.org/IC Article

Synthesis, Crystal Structure and Green Luminescence in Zero-Dimensional Tin Halide $(C_8H_{14}N_2)_2SnBr_6$

Binbin Su, Gaomin Song, Maxim S. Molokeev, Zheshuai Lin, and Zhiguo Xia*

Cite This: *Inorg. Chem.* 2020, 59, 9962–9968 Read Online

ACCESS | Metrics & More | Article Recommendations | Supporting Information

ABSTRACT: Organic–inorganic hybrid metal halides with broad-band emission are currently receiving an increasing interest for their unique light emission properties. Here we report a novel lead-free zero-dimensional (0D) tin halide, $(C_8H_{14}N_2)_2SnBr_6$, in which isolated $[SnBr_6]^{4-}$ octahedrons are cocrystallized with organic cations, 1,3-bis(aminomethyl)benzene ($C_8H_{14}N_2^{2+}$). Upon photoexcitation, the bulk crystals exhibit broad-band green emission peaking at 507 nm with a full width at half-maximum (fwhm) of 82 nm (0.395 eV), a Stokes shift of 157 nm (1.09 eV), and a photoluminescence quantum yield (PLQY) of 36 ± 4%. Combined structural analysis and density functional theory (DFT) calculations indicate that the excited state structural distortion of $[SnBr_6]^{4-}$ octahedral units account for the formation of this green emission. The relatively small Stokes shift and narrow fwhm of the emission are hence caused by the reduced distortion of $[SnBr_6]^{4-}$ octahedrons and rigid molecular structure. The discovery of lead-free $(C_8H_{14}N_2)_2SnBr_6$ and insight into the mechanism of green emission provide an essential platform toward unveiling the relationship between structure and property for 0D metal halide perovskites.

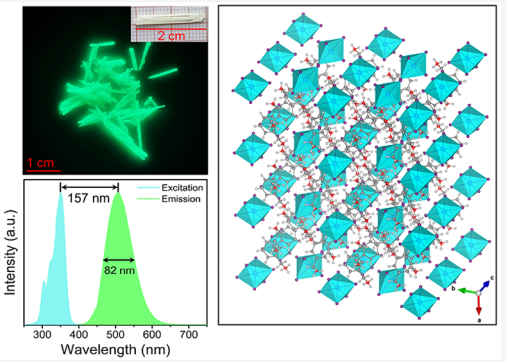

INTRODUCTION

Organic–inorganic hybrid metal halide perovskites, as a new generation of functional materials, have recently attracted extensive attention for various optoelectronic applications, such as solar cells, photodetection, light-emitting diodes, etc.[1−5] It is found that the degree of electron localization of these hybrid metal halides is closely related to the structural dimensionality: the lower the structural dimensionality, the higher the degree of electron localization.[6] Then the electronic localization culminates in zero-dimensional (0D) metal halide perovskites.[7−11] Accordingly, photoexcited electron–hole pairs are confined in metal halide polyhedron, and the appearance and following relaxation can be taken as electron transitions in central metal atoms, enabling isolated metal halide polyhedrons to exhibit inherent light emission.[12,13] 0D metal halide perovskites with ns^2 metals, such as Ge(II), Sn(II), Pb(II), and Sb(III), generally show broadband emissions with large Stokes shift, which are affected by the chemical reactivity of ns^2 ion pairs and the degree of organic cations rigidity.[6,9,14]

There exists a previous report on the 0D tin-based hybrid metal halide $(C_9NH_{20})_2SnBr_4$, of which the typical broadband emission peaking at 695 nm with a full-width at half-maximum (fwhm) of 146 nm and large Stokes shift of 332 nm is found.[15] Moreover, a variety of 0D hybrid metal halides with ns^2 metals have been developed, and their spectra cover the whole visible region and even the near-infrared region,[6,10,15−22] with the photoluminescence quantum yields (PLQY) even reaching near unity.[8] As a result, those target compounds can be regarded as remarkable candidates of highly efficient multicolor broadband emitters.[16] Recently, our group reported a 0D green-emitting compound $(C_9NH_{20})_6Pb_3Br_{12}$, peaking at about 522 nm with a fwhm of 134 nm and a large Stokes shift of 151 nm. For this phase, face-sharing $PbBr_6$ trimer clusters are cocrystallized with organic cations ($C_9NH_{20}^+$) in the 0D framework.[10] Ma and co-workers reported a new blue emitter $(C_{13}H_{19}N_4)_2PbBr_4$, peaking at 460 nm with a fwhm of 66 nm and a Stokes shift of 111 nm and the luminescence mechanisms were discussed.[9] They also reported a green emitter $(bmpy)_9[ZnCl_4]_2[Pb_3Cl_{11}]$, peaking at 512 nm with a fwhm of 61 nm and a Stokes shift of 164 nm.[20] It is of interest to note that although one can achieve multiple color broadband emissions, such as broadband green, yellow, red (deep red) and near-infrared emission, it is a challenge to obtain relatively narrow band emissions with small Stokes shifts in 0D hybrid halides, while it is important for display applications as the backlights. Moreover, the reported green-emitting 0D hybrid halides either have large Stokes shift or contain toxic Pb elements, which further limit their practical applications. Therefore, to design lead-free 0D green-emitting

Received: April 17, 2020
Published: July 6, 2020

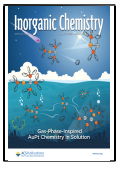

https://dx.doi.org/10.1021/acs.inorgchem.0c01103
Inorg. Chem. 2020, 59, 9962–9968

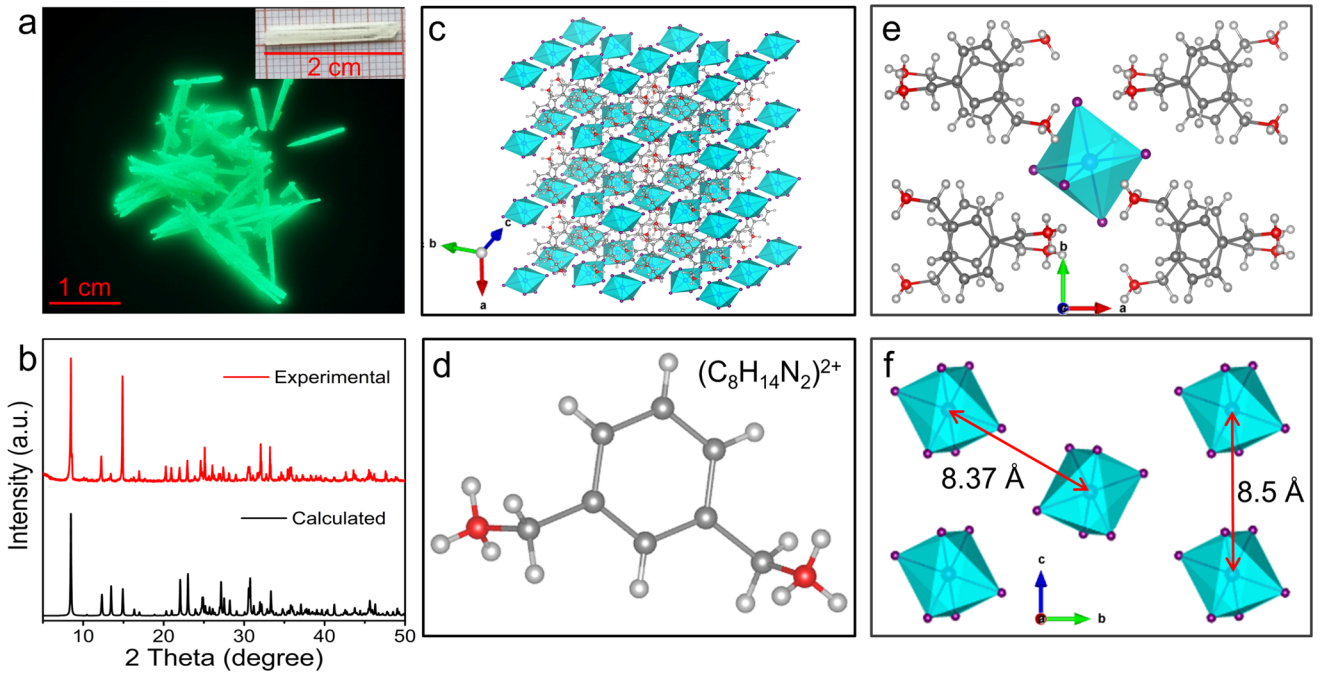

Figure 1. (a) Optical photograph of $(C_8H_{14}N_2)_2SnBr_6$ crystals under 365 nm UV irradiation and the inset shows the as-grown crystals in the daylight. (b) Calculated and experimental X-ray powder patterns of $(C_8H_{14}N_2)_2SnBr_6$. Crystal structure diagrams of 0D $(C_8H_{14}N_2)_2SnBr_6$ (c) and the organic cation $(C_8H_{14}N_2)^{2+}$ (d) (blue, tin atoms; violet, bromine atoms; red, nitrogen atoms; dark gray, carbon atoms; light gray, hydrogen atoms; sky blue polyhedron, $[SnBr_6]^{4-}$ octahedron). (e) Individual $[SnBr_6]^{4-}$ unit and nearest neighbor organic cations. (f) Schematic crystal structure along the *b* axis showing $[SnBr_6]^{4-}$ octahedrons.

hybrid halides with relatively narrow band emissions and small Stokes shifts is indispensable.

Here, we report the discovery of a new lead-free 0D hybrid metal halide $(C_8H_{14}N_2)_2SnBr_6$, which presents green emission peaking at 507 nm with a PLQY of 36 ± 4% under the excitation of 365 nm UV light. It is worth noting that this green emission shows relatively narrow fwhm of 82 nm (0.395 eV) and small Stokes shift of 157 nm (1.1 eV). The density functional theory (DFT) calculations indicate that the small excited state structural distortion accounts for the luminescence behavior. In addition, $\pi-\pi$ stacking of benzene rings in organic cations and more efficient hydrogen bonding in $(C_8H_{14}N_2)_2SnBr_6$ restrain the metal halide anions and further result in the reduced Stokes shift. As far as we know, there is no report about the green emission of 0D hybrid tin-based metal halides. Herein, the discovery of $(C_8H_{14}N_2)_2SnBr_6$ compound not only adds a new member for 0D tin-based metal halides for potential application in optoelectronic fields but also provides a fundamental principle for studying the relationship between structure and properties for 0D metal halide materials.

EXPERIMENTAL SECTION

Materials. Tin(II) bromide ($SnBr_2$, 99.9%), hydrobromic acid (HBr, 48 wt % water solution), 1,3-bis(aminomethyl)benzene, ($C_8H_{12}N_2$, 99.9%), and ethanol (C_2H_5OH, 99.8%) were purchased from Aladdin. All reagents and solvents were commercially purchased and used without further purification.

Synthesis of $(C_8H_{14}N_2)_2SnBr_6$ Polycrystalline Powder. First, 0.001 mol of $SnBr_2$ was dissolved in 15 mL of 48% HBr solution and dropwise added of 0.002 mol (1,3-bis(aminomethyl)benzene at 110 °C to form clear solution. Upon cooling to room temperature, the polycrystalline powder was separated out and repeatedly washed using ethanol. Finally, the obtained powder was dried under vacuum at 60 °C overnight.

Growth of $(C_8H_{14}N_2)_2SnBr_6$ Single Crystals. $(C_8H_{14}N_2)_2SnBr_6$ single crystals were grown in a sealed stainless-steel Parr autoclave by the programmed temperature lowering method. First, 0.001 mol $SnBr_2$ was dissolved in 15 mL 48% HBr solution at 110 °C for 5 min, followed by dropwise adding of 0.002 mol 1,3-bis(aminomethyl)-benzene to form clear solution. Subsequently, the hot solution was transferred into a preheated Teflon autoclave and then sealed in a stainless-steel Parr autoclave, which was subsequently placed in a drying oven and kept at 110 °C for 30 min. The temperature was lowered with a rate of 5.0 °C/day, and the rod-like crystals of $(C_8H_{14}N_2)_2SnBr_6$ were obtained after about 3 weeks. Finally, the obtained crystals were filtered out and washed with ethanol and dried at 60 °C overnight.

Characterization. Single-crystal X-ray diffraction (SCXRD) was conducted on a SMART APEX II X-ray single crystal diffractometers (Bruker AXS, analytical equipment of Krasnoyarsk Center of collective use of SB RAS) equipped with a CCD-detector, graphite monochromator and Mo Kα radiation (λ = 1.5406 Å) at 150 K. The absorption corrections were applied using the SADABS program. The structures were solved by the direct methods using package SHELXS and refined using the SHELXL program.[23] All the hydrogen atoms of the $C_8H_{12}N_2$ ligand were positioned geometrically as riding on their parent atoms with d(C−H) = 0.97 Å for the C−H bonds and d(N−H)=0.89 Å for all other N−H bonds and U_{iso}(H) = 1.2U_{eq}(C,N). The structural tests for the presence of missing symmetry elements and possible voids were produced using the PLATON program.[24] The supplementary crystallographic data of $(C_8H_{14}N_2)_2SnBr_6$ was provided in CCDC 1997096. Powder X-ray diffraction (PXRD) measurement was performed on a Aeris PXRD diffractometer (PANalytical Corporation, Netherlands) operating at 40 kV and 15 mA with monochromatized Cu Kα radiation (λ = 1.5406 Å). The diffuse reflection spectrum was collected by SolidSpec-3700 Shimadzu UV−vis−NIR spectrophotometer at room temperature, in which $BaSO_4$ was used as the reference standard. The photoluminescence excitation (PLE) and photoluminescence emission (PL) spectra were performed on an FLS1000 fluorescence spectrophotometer (Edinburgh Instruments Ltd., U.K.) The PLQY was recorded by an

https://dx.doi.org/10.1021/acs.inorgchem.0c01103
Inorg. Chem. 2020, 59, 9962−9968

integrated sphere, which was attached in the FLS1000 spectrofluorometer. The lifetimes were measured on an Edinburgh FLS1000 fluorescence spectrometer using a picosecond pulsed diode lasers. The dynamics of emission decay were monitored by using the FLS1000s time-correlated single-photon counting capability (1,024 channels; 1 μs window) with data collection for 5000 counts in the maximum channel.

Computational Methodology. The first-principles electronic structure was caluculated by CASTEP based on plane-wave pseudopotential density functional theory (DFT).[25] The exchange and correlation effects were carried out by the Perdew−Burke−Ernzerh (PBE) method.[26] In order to calculate the structure in the excited state, the structural optimizations based on the GGA method with PBE functional were carried. The plane-wave energy cutoff was set as 700 eV. The *k*-point separation was set as 0.07 Å^{-1} in the Brillouin zone leading to corresponding Monkhorst−Pack *k*-point meshes of 1 × 1 × 1. The lattice parameters were fixed at the experimentally measured values while the atomic positions were optimized until the force on each atom is less than 0.05 eV/Å. The more stable spin-triplet exciton is considered when calculating the excited state structure. In addition, we chose 10 electrons to transition from the ground state to the excited state and obtained the excited state structure.

RESULTS AND DISCUSSION

Figure 1a describes the optical photograph of $(C_8H_{14}N_2)_2SnBr_6$ single crystals upon the excitation of a 365 nm UV lamp, which shows bright green emission. The inset of Figure 1a demonstrates the selected $(C_8H_{14}N_2)_2SnBr_6$ crystals under ambient light and it possesses relatively large size (∼1−2 cm) and shows the body color of light green. The single crystal structure was determined, which exhibits monoclinic $P2_1/c$ symmetry with lattice parameters of a = 10.7308(3) Å, b = 14.41940(4) Å, and c = 8.50350(2) Å.

The crystallographic information file (CIF) of $(C_8H_{14}N_2)_2SnBr_6$ is demonstrated in the Supporting Information, and the main crystallographic data is given in Table 1 and

Table 1. Main Structure Parameters and Crystallographic Data of $(C_8H_{14}N_2)_2SnBr_6$

chemical formula	$C_{16}H_{28}Br_6N_4Sn$
molecular weight	874.57
temperature (K)	150
space group, Z	$P2_1/c$, 2
a (Å)	10.7308 (3)
b (Å)	14.4194 (4)
c (Å)	8.5035 (2)
β (deg)	103.570 (3)
V (Å^3)	1279.03 (6)
ρ_{calc} (g/cm^3)	2.271
$2\theta_{max}$ (deg)	58.964
$R1$ [$F_0 > 4\sigma(F_0)$]	0.0180
$wR2$	0.0342
Goof	1.047

the fractional atomic coordinates and isotropic or equivalent isotropic displacement parameters are shown in Table S1. The experimental X-ray diffraction (XRD) pattern is also in good agreement with the calculated data based on the single-crystal structure data of $(C_8H_{14}N_2)_2SnBr_6$ (Figure 1b). The crystal structures of $(C_8H_{14}N_2)_2SnBr_6$ and $(C_8H_{14}N_2)^{2+}$ are described in parts c and d of Figure 1, respectively. There are only one type of Sn site and three types of Br, and the $[SnBr_6]^{4-}$ octahedrons are isolated from each other and surrounded by bulky organic cations (Figure 1e), forming the typical 0D framework. The Sn−Br distances fall in the range of 2.9713(2) - 3.0101(2) Å (Table S2). The nearest distance between adjacent Sn ions along the b axis is about 8.37 Å (Figure 1f), indicating that there is no electronic interaction between adjacent $[SnBr_6]^{4-}$ units, as also verified by the theoretical calculation discussed below. There are six N−H···Br hydrogen bonds, and the hydrogen-bond geometries in the $(C_8H_{14}N_2)_2SnBr_6$ structure are shown in Table S3. It is worth noting that all H atoms of two NH_3 groups are involved, and these hydrogen bonds joint the $C_8H_{14}N_2$ with $[SnBr_6]^{4-}$ form 3D net (Figure S1). One can find that the more efficient hydrogen bonding can provide a constrained environment for $[SnBr_6]^{4-}$ octahedrons. In addition, the offset face-to-face $\pi-\pi$ stacking of phenyl rings in the organic molecule (Figure S2) can also improve the rigidity of the molecular structures. Thus, they help to form a relatively narrow-band emission with relatively small Stokes shift in $(C_8H_{14}N_2)_2SnBr_6$ compared with other reported 0D hybrid metal halides, as discussed below.

The photophysical properties of $(C_8H_{14}N_2)_2SnBr_6$ were investigated in detail. As shown in Figure 2a, the strongest

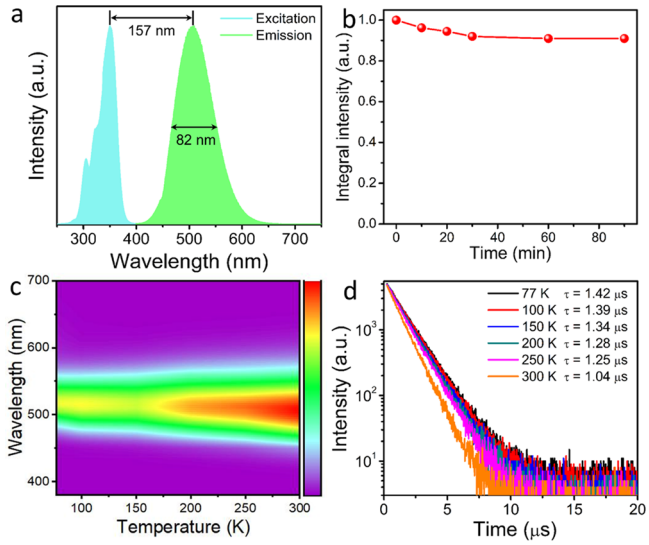

Figure 2. (a) Excitation (λ_{em} = 507 nm) and emission (λ_{ex} = 350 nm) spectra of $(C_8H_{14}N_2)_2SnBr_6$ at room temperature. (b) Photoluminescence stability of $(C_8H_{14}N_2)_2SnBr_6$ bulk crystals under continuous illumination using a 365 nm UV lamp. Temperature-dependent emission spectra (c) and decays (d) of $(C_8H_{14}N_2)_2SnBr_6$ under 350 nm excitation in the temperature range of 77−300 K.

excitation peak at 350 nm (3.54 eV) is observed in PLE spectrum. Upon the excitation at 350 nm, $(C_8H_{14}N_2)_2SnBr_6$ single crystals display green emission peaking at 507 nm with a Stokes shift of 157 nm (1.09 eV) and a fwhm of 82 nm (0.395 eV). The power density-dependent emission intensity (Figure S3) cannot reach the saturation values, indicating that this green emission band does not stem from permanent defects or doped activators.[17] We measured the excitation wavelength-dependent emission spectra at room temperature, demonstrating that the emissions remain unchanged upon excitation at different wavelengths (Figure S4). Moreover, we compared the photophysical properties of some selected 0D metal halides in the references, as shown in Table 2. For example, Cs_4SnBr_6 exhibits typical green broadband emission at 540 nm with a

https://dx.doi.org/10.1021/acs.inorgchem.0c01103
Inorg. Chem. 2020, 59, 9962−9968

Table 2. Comparison of the Photophysical Properties for Selected 0D Metal Halides

0D metal halides	emission peaks (nm)	fwhm (nm)	Stokes shift (nm)	PLQY/100%	ref
$(C_{13}H_{19}N_4)_2PbBr_4$	460	66 (0.4 eV)	111 (0.85 eV)	40	9
Cs_4SnBr_6	540	–	200(1.20 eV)	15.5	27
$(C_4N_2H_{14}Br)_4SnBr_6$	570	105	215(1.32 eV)	95	8
$(Ph_4P)_2SbCl_5$	648	136	273 (1.41 eV)	87	19
$(C_9NH_{20})_2SnBr_4$	695	146	332 (1.63 eV)	46	15
$Bmpip_2SnI_4$	730	–	317 (1.8 eV)	75	6
$(C_8H_{14}N_2)_2SnBr_6$	507	82 (0.395 eV)	157 (1.09 eV)	36 ± 4	this work

Stokes shift of 200 nm and a PLQY of 15.5%. By varying Cs or Br, the analogous compositions can be obtained, and the emission wavelengths can be changed from 500 to 620 nm.[27] Compared to all inorganic 0D metal halides, hybrid 0D metal halides not only have relatively higher PLQY with the highest value of up to 95%, but also have broader spectrum ranges, which cover the whole visible light and even near-infrared region. In this work, $(C_8H_{14}N_2)_2SnBr_6$ shows relatively narrow-band green emission with a PLQY of 36 ± 4%, and also presents excellent photostability with the integral intensities remain >90% of that at initial stage under continuous UV-light irradiation of 80 min. (Figure 2b). In addition, $(C_8H_{14}N_2)_2SnBr_6$ presents excellent air stability, and one can use and observe Sn(II) in the synthesis and the final products. As discussed above, $[SnBr_6]^{4-}$ octahedrons are protected by organic cations, so that the Sn^{2+} is hard to be oxidized to Sn^{4+}. Moreover, intermolecular interactions including hydrogen bonding and π-stacking capabilities further stabilize the oxidation resistance of Sn^{2+} ion.

Temperature-dependent emission spectra and decay curves of $(C_8H_{14}N_2)_2SnBr_6$ were investigated from 77 to 300 K (Figure 2c,d). With the temperature decreasing from 300 to 77 K, the fwhm of the corresponding emission peaks decrease from 82 nm (0.395 eV) to 59 nm (0.27 eV). Moreover, the emission peaks slightly shifted from 507 to 512 nm and the average lifetimes increase from 1.04 to 1.42 μs. It is of interest to note that the emissions also remain unchanged with the change of excitation wavelength at 77 K (Figure S5), demonstrating that the green emissions have the same luminescence mechanism in the temperature range from 77 to 300 K. The large Stokes-shifted emission and relatively long luminescence lifetime with microsecond level belong to the symbolic features of the 0D metal halide perovskites,[9,28] indicating that the emissions are attributed to the radiative relaxation of localized excitons on the isolated metal halides from the excited state to the ground state. As discussed below, this luminescence mechanism is also confirmed by the theoretical calculations.

DFT calculations were carried out to deeply analyze the electronic structures and understand the luminescence mechanisms in $(C_8H_{14}N_2)_2SnBr_6$. The flat band structure (Figure 3a) is observed, revealing the highly localized electronic states in $(C_8H_{14}N_2)_2SnBr_6$.[29] This result indicates that there is almost no electronic interaction between adjacent $[SnBr_6]^{4-}$ units, which is in consistence with previously mentioned conclusion derived from the distance of adjacent $[SnBr_6]^{4-}$ units.[8] Therefore, isolated $[SnBr_6]^{4-}$ units exhibit the intrinsic luminescence properties as found. Both the valence band maximum (VBM) and the conduction band minimum (CBM) have contributions from the localized electronic states resulting from the $[SnBr_6]^{4-}$ octahedron units, which were verified by the calculated projected density

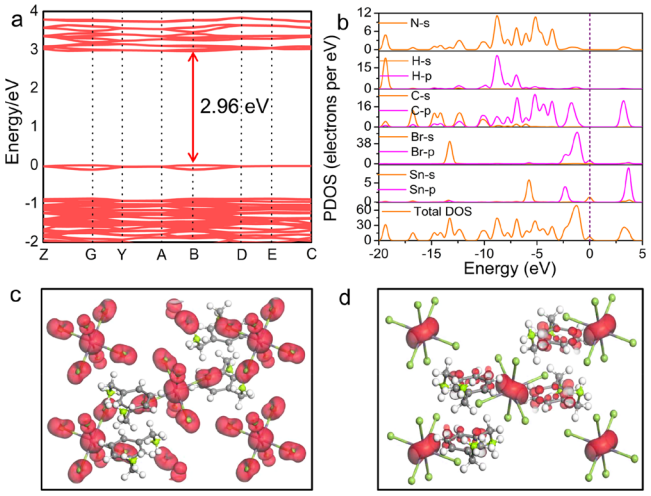

Figure 3. (a) Electronic band structure of $(C_8H_{14}N_2)_2SnBr_6$ calculated using the PBE functional. Note that the band gap is underestimated. (b) PDOS of $(C_8H_{14}N_2)_2SnBr_6$ calculated using the PBE functional. The HOMOs (c) and LUMOs (d) associated charge density maps of $(C_8H_{14}N_2)_2SnBr_6$.

of states (PDOS). As shown in Figure 3b, VBM is made up of Br-4p and Sn-6s orbitals, while the CBM is made up of mixed Sn-6p and Br-4p characters, which also agree with the other 0D tin halide perovskites.[6] In addition, the contribution of organic cations at CBM cannot be ignored, the partial PDOS on the $C_8H_{14}N_2^{2+}$ organic cations is originated from the π orbitals of phenyl rings. However, pure $C_8H_{14}N_2^{2+}$ organic cations have no photoluminescence. The partial charge density of highest occupied molecular orbitals (HOMOs) and lowest unoccupied molecular orbitals (LUMOs) are described in Figure 3c,d, indicating that the contributions of electronic states are mostly originating from inorganic $[SnBr_6]^{4-}$ octahedron units. The band gap is direct, and the PBE band gap at the B point is 2.96 eV, which is probably underestimated because of the acknowledged PBE band gap error.[10] The band gap value calculated by the diffuse reflection spectrum is 3.0 eV (Figure S6), which is in agreement with the PBE band gap.

Considering the effect of distortion degree of $[SnBr_6]^{4-}$ octahedron units on the optical properties of $(C_8H_{14}N_2)_2SnBr_6$, the geometric variations of $[SnBr_6]^{4-}$ octahedron units before and after photoexcitation have been compared to analyze their contributions (Figure 4a). In the ground state, the bond lengths between Sn^{2+} and Br^- are 2.9713 (2), 2.9926 (2), and 3.0101 (2) Å, corresponding to Sn−Br1, Sn−Br2, and Sn−Br3, respectively. The bond angles between Sn^{2+} and Br^- are 94.041, 93.869, and 97.718°, corresponding to Br1−Sn−Br2, Br2−Sn−Br3, and Br1−Sn−Br3, respectively. After photoexcitation, compared to the slightly shortened bond length of Sn−Br1 (2.9605 Å), the

https://dx.doi.org/10.1021/acs.inorgchem.0c01103
Inorg. Chem. 2020, 59, 9962−9968

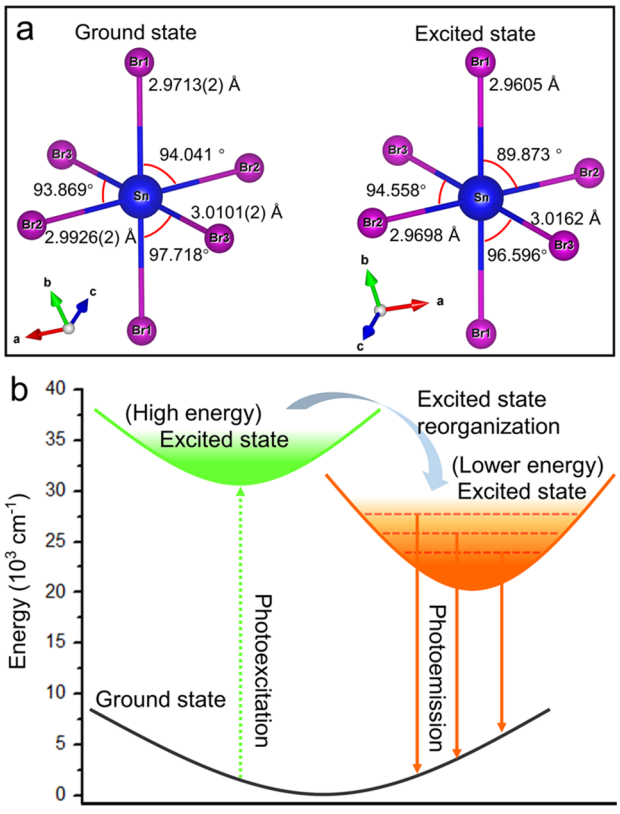

Figure 4. (a) Geometric variations of $[SnBr_6]^{4-}$ octahedron in $(C_8H_{14}N_2)_2SnBr_6$ under the optimized ground state (left) and excited state (right). (b) Schematic energy level diagram of $(C_8H_{14}N_2)_2SnBr_6$.

bond length of Sn−Br2 shortens to 2.9698 Å, while the bond length of Sn−Br3 slightly increases to 3.0162 Å. For the variation of bond angles, the Br2−Sn−Br3 slightly increases to 94.558°, and Br1−Sn−Br3 slightly decreases to 96.596°, moreover, Br1−Sn−Br2 decreases to 89.873°. The comparisons of bond lengths and bond angles before and after photoexcitation are listed in Table S4 and Table S5, respectively. The distortion degree of the $[SnBr_6]^{4-}$ octahedrons is quantitatively evaluated using eqs 1 and 2:[30]

$$\lambda_{oct} = \frac{1}{6}\sum_{i=1}^{6}[(d_i - d_0)/d_0]^2 \quad (1)$$

$$\delta^2_{oct} = \frac{1}{11}\sum_{i=1}^{12}(\theta_i - 90^\circ)^2 \quad (2)$$

where d_0 is the average Sn−Br bond length, d_i are the six individual Sn−Br bond lengths, and θ_i are the individual Br−Sn−Br bond angles of the octahedron. The λ_{oct} and $\delta_{oct}{}^2$ values of the ground state are 0.28×10^{-4} and 32, while the corresponding values in the excited state are 0.67×10^{-4} and 24 respectively. By comparing the values of λ_{oct} and $\delta_{oct}{}^2$ before and after photoexcitation, one can find that the $[SnBr_6]^{4-}$ octahedrons are slightly distorted in the excited state, which conforms to the relatively small Stokes shift for this green emission.[15] As discussed above, the more efficient hydrogen bonding and the $\pi-\pi$ stacking of benzene rings further improve the degree of organic cations rigidity, and result in a more rigid environment for $[SnBr_6]^{4-}$ octahedrons.[9] $C_8H_{14}N_2{}^{2+}$ organic cation is composed by benzene ring and methylamino, which is more rigid than that of flexible organic cations comprised of alkyl chains in 0D metal halides.[8,16] For example, the organic cations of $(C_4N_2H_{14}Br)_4SnBr_6$ are composed of soft alkyl chains without the π-stacking capabilities, which are more flexible than $C_8H_{14}N_2{}^{2+}$ organic cation. As a result, the emission of $(C_4N_2H_{14}Br)_4SnBr_6$ shows a large Stokes shift of 215 nm. And thus the combined effects from the reduced distortion of $[SnBr_6]^{4-}$ octahedrons and rigid molecular structure account for the fact that the green emission of $(C_8H_{14}N_2)_2SnBr_6$ has relatively small Stokes shift and narrow fwhm.

In general, we attribute the origin of photoluminescence to self-trapped excitons (STE) in corrugated-two-dimensional or one-dimensional structures and to molecular excited state structural reorganization (ESSR) in 0D structure with similar process.[31−33] Since the 0D metal halides possess periodic crystal structure arrangement and there is no interaction between luminescent molecular species, the photoluminescence of them is believed to originate from isolated metal halide polyhedrons, such as $[PbX_4]^{2-}$, $[SnX_6]^{4-}$, and $[SbX_5]^{2-}$.[8,9] The configuration coordinate diagram (Figure 4b) illustrated the typical photophysical processes in $(C_8H_{14}N_2)_2SnBr_6$. Under the UV photoexcitation, the $[SnBr_6]^{4-}$ octahedron units are excited from the ground state to high energy excited state, which undergoes fast excited state structural reorganization to the lower energy excited state, and then returns to ground state to generate Stokes-shifted emissions with microsecond decay times as found above.

CONCLUSIONS

In summary, we reported a novel lead-free hybrid tin-based metal halide $(C_8H_{14}N_2)_2SnBr_6$, demonstrating broad-band green emission peaking at 507 nm with a Stokes shift of 157 nm, a fwhm of 82 nm, and a PLQY of around 36 ± 4%. The detailed photophysical properties, including temperature-dependent emission spectra and decay curves, excellent photostability, and air stability have been demonstrated. The combined experimental and theoretical studies also suggest that the intermolecular interactions including hydrogen bonding and π-stacking capabilities endow $[SnBr_6]^{4-}$ octahedrons with a rigid environment, which take effect for a small Stokes shift in $(C_8H_{14}N_2)_2SnBr_6$, as further confirmed by the reduced excited state structural distortion in octahedral units. Our work not only provides a new lead-free green emission for hybrids metal halides for future emerging optoelectronic applications but also provides an essential platform to understand the relationship between structure and properties for 0D metal halide materials.

ASSOCIATED CONTENT

Supporting Information

The Supporting Information is available free of charge at https://pubs.acs.org/doi/10.1021/acs.inorgchem.0c01103.

Figures S1−S6, showing structure and photoluminescence property of the studied materials, and Tables S1−S5, providing main parameters of single crystal structure and main geometric parameters of metal halide octahedron units in the ground state and the excited state (PDF)

Accession Codes

CCDC 1997096 contains the supplementary crystallographic data for this paper. These data can be obtained free of charge via www.ccdc.cam.ac.uk/data_request/cif, or by emailing

https://dx.doi.org/10.1021/acs.inorgchem.0c01103
Inorg. Chem. 2020, 59, 9962−9968

data_request@ccdc.cam.ac.uk, or by contacting The Cambridge Crystallographic Data Centre, 12 Union Road, Cambridge CB2 1EZ, UK; fax: +44 1223 336033.

AUTHOR INFORMATION

Corresponding Author

Zhiguo Xia − *The State Key Laboratory of Luminescent Materials and Devices, Guangdong Provincial Key Laboratory of Fiber Laser Materials and Applied Techniques, School of Materials Science and Technology, South China University of Technology, Guangzhou 510640, P. R. China;* orcid.org/0000-0002-9670-3223; Email: xiazg@scut.edu.cn

Authors

Binbin Su − *The State Key Laboratory of Luminescent Materials and Devices, Guangdong Provincial Key Laboratory of Fiber Laser Materials and Applied Techniques, School of Materials Science and Technology, South China University of Technology, Guangzhou 510640, P. R. China*

Gaomin Song − *Technical Institute of Physics and Chemistry, University of Chinese Academy of Sciences, Beijing 100190, P. R. China;* orcid.org/0000-0001-5535-0188

Maxim S. Molokeev − *Laboratory of Crystal Physics, Kirensky Institute of Physics, Federal Research Center KSC SB RAS, Krasnoyarsk 660036, Russia; Siberian Federal University, Krasnoyarsk 660041, Russia; Department of Physics, Far Eastern State Transport University, Khabarovsk 680021, Russia*

Zheshuai Lin − *Technical Institute of Physics and Chemistry, University of Chinese Academy of Sciences, Beijing 100190, P. R. China;* orcid.org/0000-0002-9829-9893

Complete contact information is available at: https://pubs.acs.org/10.1021/acs.inorgchem.0c01103

Notes

The authors declare no competing financial interest.

ACKNOWLEDGMENTS

This work is supported by the National Natural Science Foundation of China (51961145101, 51722202, and 51972118), Fundamental Research Funds for the Central Universities (D2190980), Guangzhou Science & Technology Project (202007020005), and the Guangdong Provincial Science & Technology Project (No. 2018A050506004), and the Local Innovative and Research Teams Project of Guangdong Pearl River Talents Program (2017BT01X137). This work is also funded by RFBR according to Research Project No. 19-52-80003.

REFERENCES

(1) Zhou, G. J.; Su, B. B.; Huang, J. L.; Zhang, Q. Y.; Xia, Z. G. Broad-Band Emission in Metal Halide Perovskites: Mechanism, Materials, and Applications. *Mater. Sci. Eng., R* **2020**, *141*, 100548.

(2) Chen, K.; Schunemann, S.; Song, S.; Tuysuz, H. Structural Effects on Optoelectronic Properties of Halide Perovskites. *Chem. Soc. Rev.* **2018**, *47* (18), 7045−7077.

(3) Shan, Q. S.; Song, J. Z.; Zou, Y. S.; Li, J. H.; Xu, L. M.; Xue, J.; Dong, Y. H.; Han, B. N.; Chen, J. W.; Zeng, H. B. High Performance Metal Halide Perovskite Light-Emitting Diode: From Material Design to Device Optimization. *Small* **2017**, *13* (45), 1701770.

(4) Stranks, S. D.; Snaith, H. J. Metal-Halide Perovskites for Photovoltaic and Light-Emitting Devices. *Nat. Nanotechnol.* **2015**, *10*, 391.

(5) Zhang, Y. P.; Liu, J. Y.; Wang, Z. Y.; Xue, Y. Z.; Ou, Q. D.; Polavarapu, L.; Zheng, J. L.; Qi, X.; Bao, Q. L. Synthesis, Properties, and Optical Applications of Low-Dimensional Perovskites. *Chem. Commun.* **2016**, *52* (94), 13637−13655.

(6) Morad, V.; Shynkarenko, Y.; Yakunin, S.; Brumberg, A.; Schaller, R. D.; Kovalenko, M. V. Disphenoidal Zero-Dimensional Lead, Tin, and Germanium Halides: Highly Emissive Singlet and Triplet Self-Trapped Excitons and X-ray Scintillation. *J. Am. Chem. Soc.* **2019**, *141* (25), 9764−9768.

(7) Benin, B. M.; Dirin, D. N.; Morad, V.; Worle, M.; Yakunin, S.; Raino, G.; Nazarenko, O.; Fischer, M.; Infante, I.; Kovalenko, M. V. Highly Emissive Self-Trapped Excitons in Fully Inorganic Zero-Dimensional Tin Halides. *Angew. Chem., Int. Ed.* **2018**, *57* (35), 11329−11333.

(8) Zhou, C. K.; Lin, H. R.; Tian, Y.; Yuan, Z.; Clark, R.; Chen, B. H.; van de Burgt, L. J.; Wang, J. C.; Zhou, Y.; Hanson, K.; Meisner, Q. J.; Neu, J.; Besara, T.; Siegrist, T.; Lambers, E.; Djurovich, P.; Ma, B. W. Luminescent Zero-Dimensional Organic Metal Halide Hybrids with Near-Unity Quantum Efficiency. *Chem. Sci.* **2018**, *9* (3), 586−593.

(9) Lin, H. R.; Zhou, C. K.; Chaaban, M.; Xu, L. J.; Zhou, Y.; Neu, J.; Worku, M.; Berkwits, E.; He, Q.; Lee, S.; Lin, X. S.; Siegrist, T.; Du, M. H.; Ma, B. W. Bulk Assembly of Zero-Dimensional Organic Lead Bromide Hybrid with Efficient Blue Emission. *ACS Mater. Lett.* **2019**, *1* (6), 594−598.

(10) Zhou, J.; Li, M. Z.; Ning, L. X.; Zhang, R. L.; Molokeev, M. S.; Zhao, J.; Yang, S. Q.; Han, K. L.; Xia, Z. G. Broad-Band Emission in a Zero-Dimensional Hybrid Organic $[PbBr_6]$ Trimer with Intrinsic Vacancies. *J. Phys. Chem. Lett.* **2019**, *10* (6), 1337−1341.

(11) Mohammed, O. F. Outstanding Challenges of Zero-Dimensional Perovskite Materials. *J. Phys. Chem. Lett.* **2019**, *10* (19), 5886−5888.

(12) Vogler, A.; Nikol, H. The Structures of s^2 Metal Complexes in the Ground and sp Excited States. *Comments Inorg. Chem.* **1993**, *14*, 245−261.

(13) Almutlaq, J.; Yin, J.; Mohammed, O. F.; Bakr, O. M. The Benefit and Challenges of Zero-Dimensional Perovskites. *J. Phys. Chem. Lett.* **2018**, *9* (14), 4131−4138.

(14) Shi, H. l.; Han, D.; Chen, S. y.; Du, M. H. Impact of Metal ns^2 Lone Pair on Luminescence Quantum Efficiency in Low-Dimensional Halide Perovskites. *Phys. Rev. Mater.* **2019**, *3*, 034604.

(15) Zhou, C. K.; Lin, H. R.; Shi, H. L.; Tian, Y.; Pak, C.; Shatruk, M.; Zhou, Y.; Djurovich, P.; Du, M. H.; Ma, B. W. A Zero-Dimensional Organic Seesaw-Shaped Tin Bromide with Highly Efficient Strongly Stokes-Shifted Deep-Red Emission. *Angew. Chem., Int. Ed.* **2018**, *57* (4), 1021−1024.

(16) Zhou, C. K.; Tian, Y.; Yuan, Z.; Lin, H. R.; Chen, B. H.; Clark, R.; Dilbeck, T.; Zhou, Y.; Hurley, J.; Neu, J.; Besara, T.; Siegrist, T.; Djurovich, P.; Ma, B. W. Highly Efficient Broadband Yellow Phosphor Based on Zero-Dimensional Tin Mixed-Halide Perovskite. *ACS Appl. Mater. Interfaces* **2017**, *9* (51), 44579−44583.

(17) Zhou, L.; Liao, J. F.; Huang, Z. G.; Wei, J. H.; Wang, X. D.; Chen, H. Y.; Kuang, D. B. Intrinsic Self-Trapped Emission in 0D Lead-Free $(C_4H_{14}N_2)_2In_2Br_{10}$ Single Crystal. *Angew. Chem., Int. Ed.* **2019**, *58* (43), 15435−15440.

(18) Zhou, C. K.; Lin, H. R.; Worku, M.; Neu, J.; Zhou, Y.; Tian, Y.; Lee, S.; Djurovich, P.; Siegrist, T.; Ma, B. W. Blue Emitting Single Crystalline Assembly of Metal Halide Clusters. *J. Am. Chem. Soc.* **2018**, *140* (41), 13181−13184.

(19) Zhou, C. K.; Worku, M.; Neu, J.; Lin, H. R.; Tian, Y.; Lee, S.; Zhou, Y.; Han, D.; Chen, S. Y.; Hao, A.; Djurovich, P. I.; Siegrist, T.; Du, M. H.; Ma, B. W. Facile Preparation of Light Emitting Organic Metal Halide Crystals with Near-Unity Quantum Efficiency. *Chem. Mater.* **2018**, *30* (7), 2374−2378.

(20) Zhou, C. K.; Lin, H. R.; Neu, J.; Zhou, Y.; Chaaban, M.; Lee, S.; Worku, M.; Chen, B. H.; Clark, R.; Cheng, W. H.; Guan, J. J.; Djurovich, P.; Zhang, D. Z.; Lu, X. J.; Bullock, J.; Pak, C.; Shatruk, M.; Du, M. H.; Siegrist, T.; Ma, B. W. Green Emitting Single-Crystalline Bulk Assembly of Metal Halide Clusters with Near-Unity Photo-

luminescence Quantum Efficiency. *ACS Energy Lett.* **2019**, *4* (7), 1579−1583.
(21) Li, M. Z.; Zhou, J.; Zhou, G. J.; Molokeev, M. S.; Zhao, J.; Morad, V.; Kovalenko, M. V.; Xia, Z. G. Hybrid Metal Halides with Multiple Photoluminescence Centers. *Angew. Chem., Int. Ed.* **2019**, *58* (51), 18670−18675.
(22) Jun, T.; Sim, K.; Iimura, S.; Sasase, M.; Kamioka, H.; Kim, J.; Hosono, H. Lead-Free Highly Efficient Blue-Emitting $Cs_3Cu_2I_5$ with 0D Electronic Structure. *Adv. Mater.* **2018**, *30* (43), 1804547.
(23) Sheldrick, G. M. Crystal Structure Refinement with SHELXL. *Acta Crystallogr., Sect. C: Struct. Chem.* **2015**, *71*, 3−8.
(24) Spek, A. L. *PLATON - A Multipurpose Crystallographic Tool*; Utrecht University: Utrecht, The Netherlands, 2008.
(25) Clark, S. J.; Segall, M. D.; Pickard, C. J.; Hasnip, P. J.; Probert, M. I. J.; Refson, K. P.M. First principles methods using CASTEP. *Z. Kristallogr. - Cryst. Mater.* **2005**, *220* (5−6), 567−570.
(26) Ceperley, D. M.; Alder, B. J. Ground State of the Electron Gas by a Stochastic Method. *Phys. Rev. Lett.* **1980**, *45* (7), 566.
(27) Benin, B. M.; Dirin, D. N.; Morad, V.; Wörle, M.; Yakunin, S.; Rainò, G.; Nazarenko, O.; Fischer, M.; Infante, I.; Kovalenko, M. V. Highly Emissive Self-Trapped Excitons in Fully Inorganic Zero-Dimensional Tin Halides. *Angew. Chem., Int. Ed.* **2018**, *57* (35), 11329−11333.
(28) Yu, J. C.; Kong, J. T.; Hao, W.; Guo, X. T.; He, H. J.; Leow, W. R.; Liu, Z. Y.; Cai, P. Q.; Qian, G. D.; Li, S. Z.; Chen, X. Y.; Chen, X. D. Broadband Extrinsic Self-Trapped Exciton Emission in Sn-Doped 2D Lead-Halide Perovskites. *Adv. Mater.* **2018**, *31* (7), 1806385.
(29) Ju, M. G.; Dai, J.; Ma, L.; Zeng, X. C. Lead-Free Mixed Tin and Germanium Perovskites for Photovoltaic Application. *J. Am. Chem. Soc.* **2017**, *139* (23), 8038−8043.
(30) Yangui, A.; Pillet, S.; Bendeif, E.-E.; Lusson, A.; Triki, S.; Abid, Y.; Boukheddaden, K. Broadband Emission in a New Two-Dimensional Cd-Based Hybrid Perovskite. *ACS Photonics* **2018**, *5* (4), 1599−1611.
(31) Dohner, E. R.; Jaffe, A.; Bradshaw, L. R.; Karunadasa, H. I. Intrinsic White-Light Emission from Layered Hybrid Perovskites. *J. Am. Chem. Soc.* **2014**, *136*, 13154−13157.
(32) Cortecchia, D.; Neutzner, S.; Srimath Kandada, A. R.; Mosconi, E.; Meggiolaro, D.; De Angelis, F.; Soci, C.; Petrozza, A. Broadband Emission in Two-Dimensional Hybrid Perovskites: The Role of Structural Deformation. *J. Am. Chem. Soc.* **2017**, *139* (1), 39−42.
(33) Kovalenko, M.; Protesescu, L.; Bodnarchuk, M. Properties and Potential Optoelectronic Applications of Lead Halide Perovskite Nanocrystals. *Science* **2017**, *358*, 745−750.

https://dx.doi.org/10.1021/acs.inorgchem.0c01103
Inorg. Chem. 2020, 59, 9962−9968